



On the Influence of Thermal History on the Martensitic Transformation in Ti-24Nb-4Zr-8Sn (wt%)

N. L. Church¹ · C. E. P. Talbot¹ · N. G. Jones¹

Received: 23 June 2020 / Revised: 18 December 2020 / Accepted: 23 December 2020 / Published online: 16 February 2021
© The Author(s) 2021

Abstract Metastable β titanium alloys, such as Ti-24Nb-4Zr-8Sn, have potential for application in vibration damping systems due to their ability to display superelastic behaviour. However, their use is currently limited due to large variations in the temperature range over which this behaviour is stable, which can additionally be shown to depend on the thermal history of the sample. This study demonstrates the sensitivity of the microstructure to thermal history and highlights a possible cause for this variability. Currently held theories of ω formation suppressing the martensitic transformation have been called into question and an alternative mechanism based on a total stress approach has been suggested. Understanding this variability enables better design of alloys and processing routes in order to achieve materials with the desired properties required for industrial application.

Keywords Superelasticity · Thermal cycling · Transformation temperature · TiNb alloys

Introduction

Metastable β titanium alloys have received considerable attention for engineering applications due to their ability to recover large strains through superelastic behaviour. This feature combined with a high specific strength, good corrosion resistance and excellent biocompatibility has made

them attractive candidates for both aerospace and biomedical industries as an alternative to NiTi [1, 2].

When loading superelastic Ti alloys, the parent bcc β phase shears to form the orthorhombic α'' martensite once a critical stress has been reached (σ_{SIM}), giving rise to macroscopic strain. When the load is removed, the reverse transformation occurs, restoring the β phase and recovering the strains associated with the change in crystal structure. The reversibility of this transformation is only possible if a thermodynamic driving force exists, meaning that the β phase must be more thermodynamically stable than the α'' phase at the testing temperature. Consequently, the thermal onset temperature of the martensitic transformation (M_s) must also be below this temperature. Within the related literature for NiTi, defect concentration is often reported to affect the M_s temperature [3–5]; however, in solution heat-treated samples, the composition is believed to be the dominant factor that determines M_s . For β TiNb alloys, composition is also recognised as an important factor in determining M_s , with the effect of alloying additions often being well reported within the literature [6–8]. Therefore, it follows that for solution-treated samples of TiNb-based alloys of identical composition, M_s should be approximately constant.

However, a difference between the observed M_s temperature for TiNb samples of identical composition was noted when cooled from the β phase field at different rates [9]. This difference was attributed to ω precipitation on cooling, which was reported to be more pronounced during slower cooling. ω exists in two different forms: isothermal (ω_{iso}), which forms via a diffusion-based mechanism, and athermal (ω_{ath}), which forms without diffusion. As ω_{iso} results in atomic rearrangements, the β matrix is enriched in β stabilising elements and this has been suggested as a mechanism by which it can suppress α'' phase formation

✉ N. G. Jones
ngj22@cam.ac.uk

¹ Department of Materials Science and Metallurgy, University of Cambridge, 27 Charles Babbage Road, Cambridge CB3 0FS, UK

[10, 11]. However, as the ω_{ath} variant is compositionally identical to the β phase, it cannot suppress the martensitic transformation by the same mechanism. α'' competition with ω_{iso} can rationalise the effects seen for some alloys aged for long periods [12, 13]. However, given the need for diffusional processes, questions have been raised in relation to the time period necessary for ω_{iso} to form when considering material that has been cooled at intermediate rates [14]. As such, it is believed that in materials cooled at intermediate rates, such as those achieved when air cooling samples with small dimensions, it will be ω_{ath} rather than ω_{iso} that forms [9].

Observations of a M_s temperature not linked solely to compositional variations have been made in other TiNb alloys. Differential Scanning Calorimetry (DSC) performed on Ti-Nb-Sn alloys identified a difference in the onset of the martensitic transformation between samples that were air cooled, oil quenched and ice-water quenched [15]. In addition, DSC data from a number of Ti-Nb-Mo alloys heated to different peak temperatures indicated a decrease in M_s when the peak temperature was higher [16]. Both of these studies attributed this effect to the precipitation of ω_{iso} . More recently, a study into the effects of cooling rate on Ti24Nb (at.%) identified a difference in the constituent phases between two slightly different cooling rates [14]. However, the difference in time spent in the fast ω_{iso} precipitation window was not believed to have been sufficient in order to account for the observed differences in phase fractions. Furthermore, in samples cooled slowly from the β phase field to room temperature, no thermal transformation was observed when the temperature was reduced further to -168 °C, demonstrating that M_s must be below this temperature for the alloy in this condition. In contrast, samples of identical composition cooled quickly from the β phase field to room temperature demonstrated a reversible martensitic transformation with a published M_s temperature of 115 °C [14]. This is a difference in reported M_s temperature of almost 300 °C.

Therefore, although current theory inferring M_s is fixed for solution-treated alloys of identical composition, a difference in cooling method has been observed to affect M_s . This has been rationalised as an effect of α'' competition with ω , where one forms to the exclusion of the other at different cooling rates [9]. However, ω_{iso} is not necessarily thought to be able to form within these timeframes. Furthermore, there is limited evidence to suggest that ω_{ath} has a significant effect on the propensity for α'' to form, with some studies observing α'' and ω_{ath} together in the same microstructure after quenching [17, 18], and many others showing a stress-induced α'' transformation is still possible in a $\beta + \omega_{\text{ath}}$ microstructure [19–23].

Such large variations in the observed M_s temperature for this class of alloys requires further investigation if they are

to be successfully deployed in engineering applications. In particular, the role of the ω phase requires further elucidation. To identify whether ω is having an effect on the M_s temperature in alloys of this type, the behaviour of an alloy less susceptible to its formation must be considered.

Ti-24Nb-4Zr-8Sn wt% (Ti2448) is a commercial alloy designed with a high Sn content that is believed to completely suppress the ω transformation [24]. Ti2448 has the ability to achieve recoverable strains on the order of 2%; however, with specific processing conditions this can be increased to as high as 3% [19, 25–29]. The related literature suggests that M_s lies close to -50 °C for this alloy [30, 31], however, there have been reports of M_s as low as -200 °C [28, 32], with a refined grain size cited as the underlying factor in influencing the M_s temperature in this case. Furthermore, cyclically loaded specimens of Ti2448 at varying temperatures demonstrated superelastic recovery at temperatures as low as 4.2 K [33]. Due to the requirement that the β phase must be the more thermodynamically stable phase in order to observe superelastic recovery, it was concluded that there was no thermally driven transformation. i.e. M_s must in fact be < -268 °C; over 200 °C lower than the commonly reported value. The same authors also observed superelastic recovery at room temperature (23 °C) suggesting a very large temperature range over which these alloys can be utilised.

This work aims to investigate the effect of cooling method and subsequent thermal cycling on Ti2448 to provide insights into the mechanisms that influence the transformation behaviour of this alloy.

Methods

A commercially produced plate of Ti2448, 2 mm in thickness, was cut into approximately 1 cm² samples for investigation. The composition of the material was determined by a certified external laboratory, using X-ray fluorescence (XRF) spectroscopy for the metallic elements and LECO analysis for the interstitial elements, carbon, nitrogen and oxygen.

Prior to any heat treatment, samples were wrapped in Ta foil and encapsulated in evacuated quartz ampoules. Samples were then subjected to a solution heat treatment of 900 °C for 30 min followed by cooling at three different rates: (i) a fast water quench (FWQ)—cooling in ice-water and smashing the ampoule; (ii) a slow water quench (SWQ)—cooling in ice-water while leaving the ampoule intact; or (iii) air cooling (AC)—cooled in ambient laboratory air within the quartz ampoule.

Samples in all three conditions were prepared for subsequent analysis by first grinding using 15 μm SiC papers. Laboratory X-ray diffraction (XRD) was performed on a

Bruker D8 Advance with a LynxEye EX position sensitive detector, using Cu-K α radiation, a 2θ range of 30–100° in increments of 0.02°, a variable slit width, fixed sample illumination of 10 mm and a 1 s time step.

These samples were subsequently polished using 0.04 μm colloidal silica, buffered to pH 7. Critically, samples were not mounted in resin during the preparation process so as to avoid any potential thermal effects when curing the mounting material.

To assess the microstructure, electron channelling contrast imaging (ECCI) and electron back scattered diffraction (EBSD) were performed using a Zeiss GeminiSEM 300. ECCI micrographs were obtained using a BSD detector, a 30 μm aperture and an accelerating voltage of 15 kV. EBSD patterns were acquired using a 120 μm aperture and an accelerating voltage of 25 kV by an Oxford Instruments Symmetry detector set to a dwell time of 20 ms and a step size of 2.5 μm . Inverse pole figure (IPF) maps, along with grain diameters, were generated using the Channel 5 Tango software. Pole figures were produced using the Channel 5 Mambo software. The standard error (SE) and standard deviation (σ_{SD}) were calculated for each sample, using the grain diameters identified by the software. Due to the similarity of the Kikuchi patterns for the β and α'' phases, in addition to the fine scale of the α'' variants and the quality of the patterns obtained, unambiguous attribution of each set of Kikuchi bands to a single phase was unreliable. However, the close correspondence of the patterns and the known orientation relationship between the two phases allowed each image to be successfully indexed if only the β phase was considered. This approach enabled the prior parent β grain size and orientation to be determined for each sample, regardless of α'' volume fraction. The grain boundaries in the maps reconstructed in this manner were always directly correlated with delineations in the corresponding band contrast image.

Transmission electron microscopy (TEM) samples were thinned to electron transparency through a standard focussed ion beam (FIB) lift-out method using an FEI Helios NanoLab 600 DualBeam FIB. Selected area diffraction (SAD) patterns and high-angle annular dark field (HAADF) images along with accompanying scanning transmission electron microscopy energy dispersive X-ray spectroscopy (STEM-EDX) elemental maps were obtained from the centres of each sample using an FEI Osiris TEM, equipped with Super-X EDX detectors, operated at 200 kV.

Differential Scanning Calorimetry (DSC) experiments were performed on 3 mm diameter discs that were spark eroded from samples in each condition. Heat flow data were acquired using a TA Q2000 with a heating and cooling rate of 10 $^{\circ}\text{C min}^{-1}$. Samples were first equilibrated at 20 $^{\circ}\text{C}$ and then heated to 200 $^{\circ}\text{C}$ before being

cooled to -60 $^{\circ}\text{C}$. They were then thermally cycled from -60 $^{\circ}\text{C}$ to progressively higher peak temperatures (250 $^{\circ}\text{C}$, 300 $^{\circ}\text{C}$ and 350 $^{\circ}\text{C}$). A sample in the FWQ condition was then subjected to five thermal cycles between -60 $^{\circ}\text{C}$ and a peak temperature of 250 $^{\circ}\text{C}$. Thermal onset temperatures were determined by the intersection of the extrapolated baseline with the steepest tangent lines to the peaks.

Results

Initial Microstructure

The measured composition of the alloy in the AC condition is presented in Table 1. This composition was close to the nominal of Ti2448, with a low oxygen content when compared to reported literature values [25, 30, 34–36]. No significant variation in the oxygen content was expected between material in the AC and the SWQ conditions, as both were prepared in an identical fashion, and the quartz ampoules remained intact until the samples were fully cooled to room temperature. In contrast, the FWQ condition showed evidence of an oxide on the surface following quenching, presumably due to the high sample temperature when contact was made with the water. Since oxygen is widely reported to suppress the martensitic transformation any modification to the transformation behaviour of this sample as a result of oxygen pick-up during processing would be most pronounced in the FWQ sample [37].

The microstructural condition of samples subjected to the three different cooling rates is presented in Fig. 1. The AC and SWQ samples comprised of recrystallised grains of β on the order of 40 μm . By contrast, there was evidence of lenticular structures within the β grains of the FWQ condition, believed to be the martensitic α'' phase.

To confirm the phases present in these microstructures, XRD patterns were acquired, as shown in Fig. 2. Strong β reflections were present in the traces of all three conditions. Additional peaks consistent with the martensitic α'' phase were present in the SWQ and FWQ conditions, being much more pronounced in the latter. Taking peak area as a proxy to volume fraction, this demonstrated a significant amount

Table 1 Measured composition of the alloy after solution heat treatment and AC

Ti	Nb	Zr	Sn	O	N	C
Bal	24.19	3.72	7.29	0.079	0.008	0.012

Ti, Nb, Zr and Sn are given in wt%, whereas O, N and C are given in weight ppm

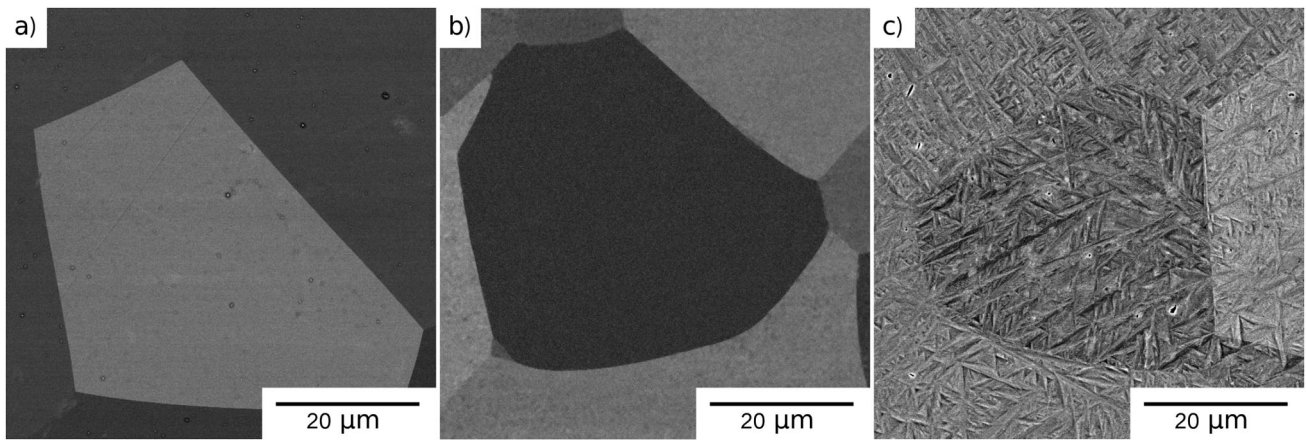


Fig. 1 Channelling contrast SEM micrographs of the **a** AC **b** SWQ and **c** FWQ conditions

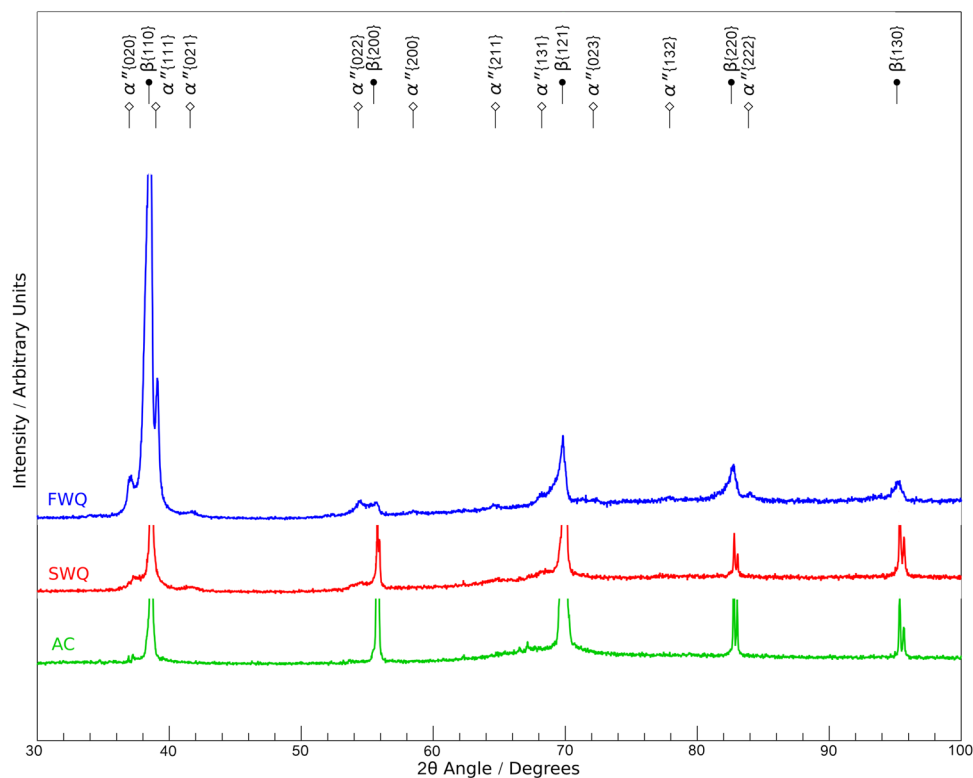


Fig. 2 Lab-based XRD patterns for samples in the AC, SWQ and FWQ conditions

of α'' present in the FWQ condition, which was consistent with the results presented in Fig. 1.

As the presence of the ω phase is often not discernible by lab-based XRD methods, further investigation was performed using TEM. SAD patterns were obtained for the two microstructural extremes (AC and FWQ) when aligned along the $[\bar{1}13]_{\beta}$. These data are shown in Fig. 3. In the AC condition, intense diffraction spots consistent with the β phase were observed, along with weak spots corresponding

to the ω phase at $1/3$ and $2/3$ $\langle 112 \rangle_{\beta}$. Between these ω reflections, at $1/2$ $\langle 112 \rangle_{\beta}$, very weak spots could be seen, which may indicate the presence of a small fraction of α'' martensite. However, given the absence of this phase in both the XRD patterns and the ECCI images, then if present in the TEM sample, it is likely that this martensite formed during preparation of the foil. In the FWQ condition, strong β reflections were also observed, but, in this

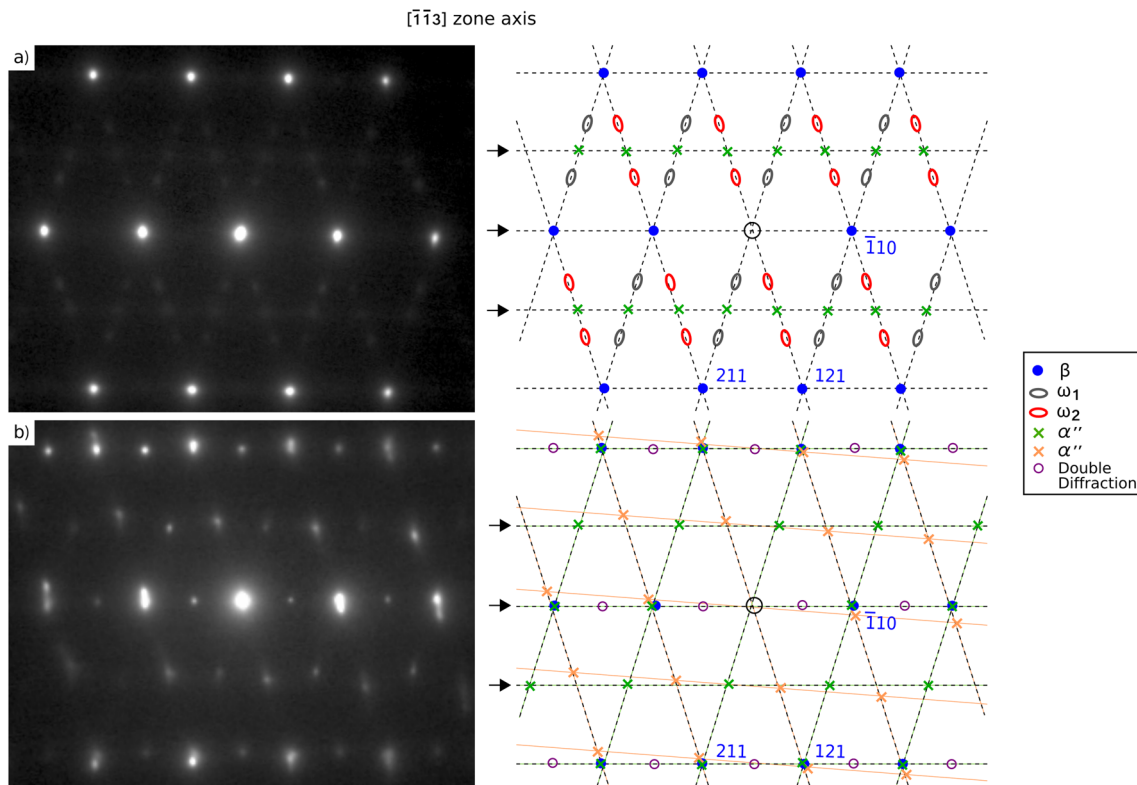


Fig. 3 TEM SAD patterns from a $[113]$ zone axis and accompanying key diagram for **a** AC and **b** FWQ conditions

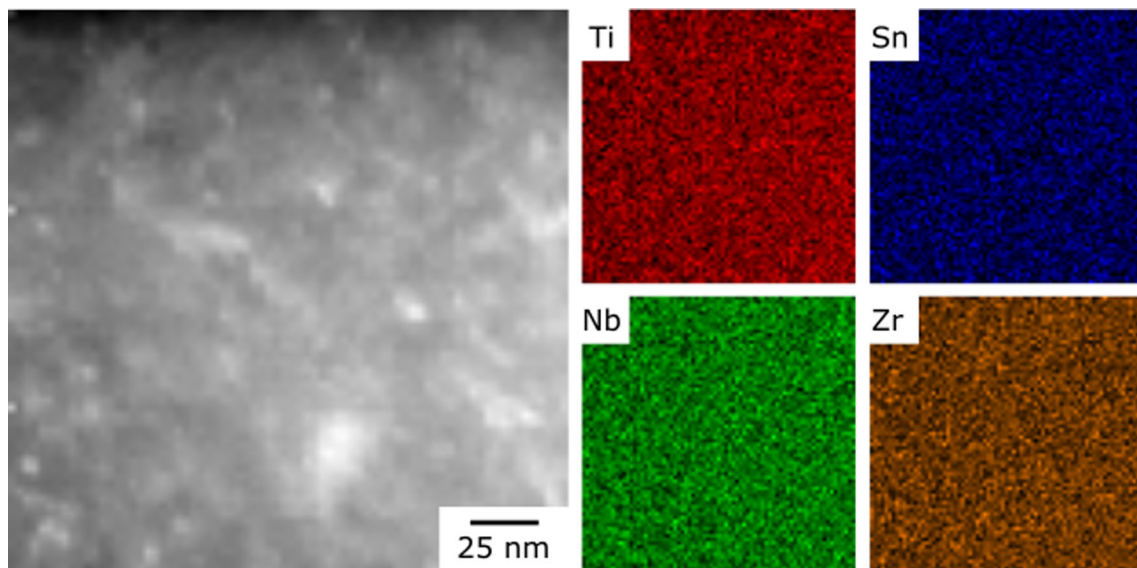


Fig. 4 HAADF image and STEM-EDX elemental distribution maps for Ti2448 in the AC condition

case, there were additional intense reflections consistent with α'' martensite along the $\langle 112 \rangle_{\alpha''}$ zone axis.

To ascertain whether the ω spots observed in the AC condition related to the ω_{ath} or the ω_{iso} form of this phase, HAADF images were obtained along with corresponding STEM-EDX compositional maps. These data are presented

in Fig. 4. Within the HAADF image, small regions with brighter contrast could be observed. However, no corresponding variations in composition were revealed in the EDX data. Instead, the STEM-EDX maps, which were acquired with nm resolution, revealed an even distribution for all of the constituent elements, implying a

compositionally homogenous material. Consequently, in the absence of compositionally distinct, Ti-enriched precipitates, it can only be concluded that the ω present in the microstructure was the ω_{ath} form.

Previous work has linked grain refinement below $\sim 40 \mu\text{m}$ to a decrease in M_s of these alloys [38]; however, much smaller grain sizes between 200 and 50 nm have been required to have a more dramatic effect on M_s [28, 32]. Therefore, the grain size and texture of the alloy

in each of the three different cooling conditions were characterised by EBSD. These results are presented in Fig. 5, with average grain sizes of the AC, SWQ and FWQ samples of $68.0 \pm 1.4 \mu\text{m}$ ($\sigma_{\text{SD}} = 35 \mu\text{m}$), $73 \pm 2 \mu\text{m}$ ($\sigma_{\text{SD}} = 43 \mu\text{m}$) and $81 \pm 2 \mu\text{m}$ ($\sigma_{\text{SD}} = 46 \mu\text{m}$), respectively. Consequently, it can be seen that grain size did not significantly vary between the three conditions, and a grain size below $40 \mu\text{m}$, where M_s has been shown to be affected, has not been achieved. The texture of all three

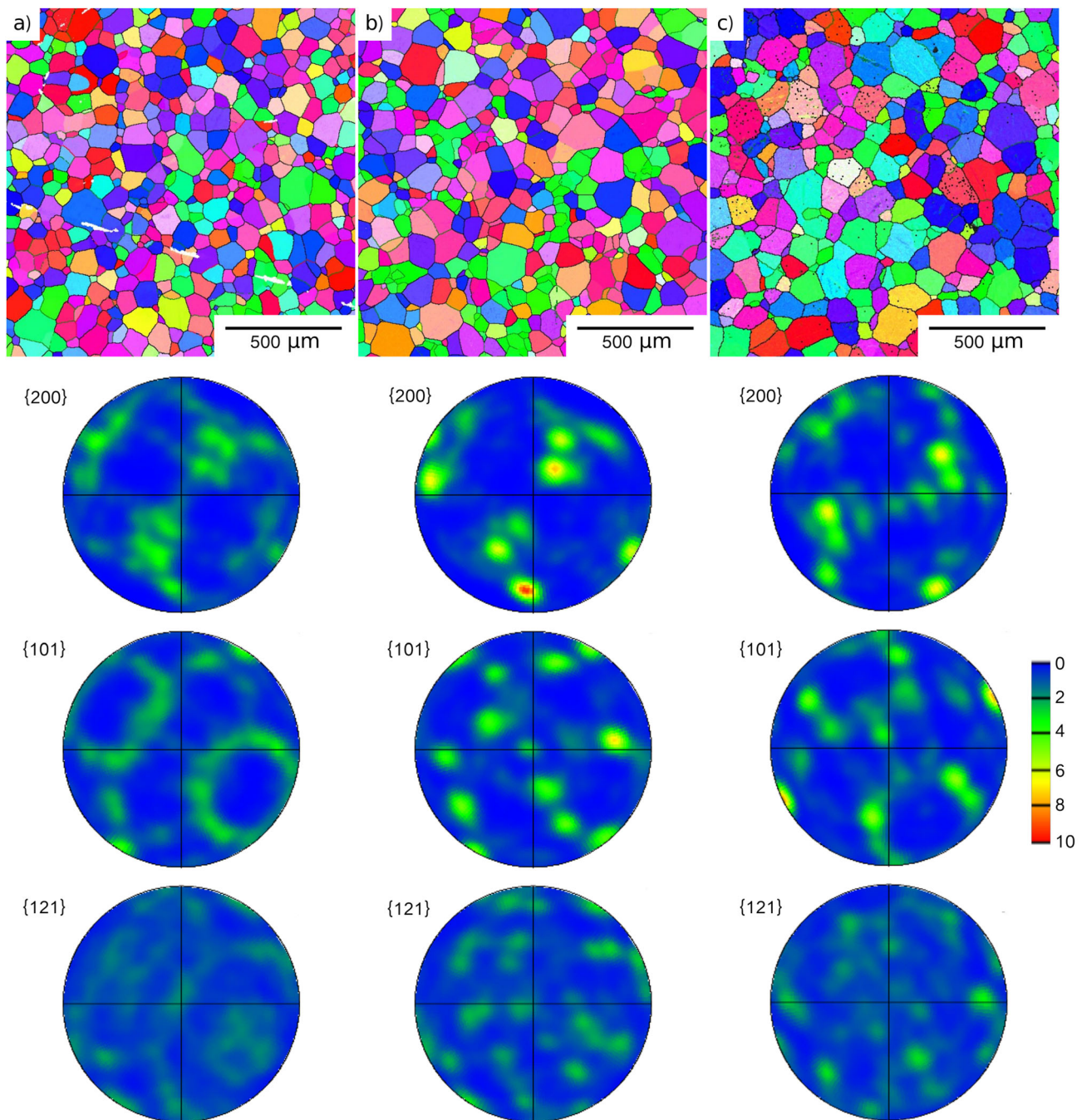


Fig. 5 EBSD IPF-Z maps showing grain size, with associated pole figures showing texture for the **a** AC, **b** SWQ and **c** FWQ conditions

conditions was relatively low compared to the recrystallised and cold rolled textures reported in the literature [39]. The AC condition has the smallest degree of texture of the three. The SWQ and FWQ are comparable; however, the latter has a slightly weaker texture. Therefore, the differences in texture of the three conditions show no trend and are most likely to be a result of the specific areas of the sample from which the data were collected, along with sample-to-sample variation. The observed difference in phase composition of these three conditions must, therefore, be independent of composition, grain size and texture.

The Effect of Thermal Cycling

To identify M_s for the SWQ and FWQ conditions, DSC thermograms were obtained by heating samples to 200 °C in order to transform the α'' to β and then cooled to -60 °C to allow the α'' to reform. The corresponding thermogram for the two quenched conditions is presented

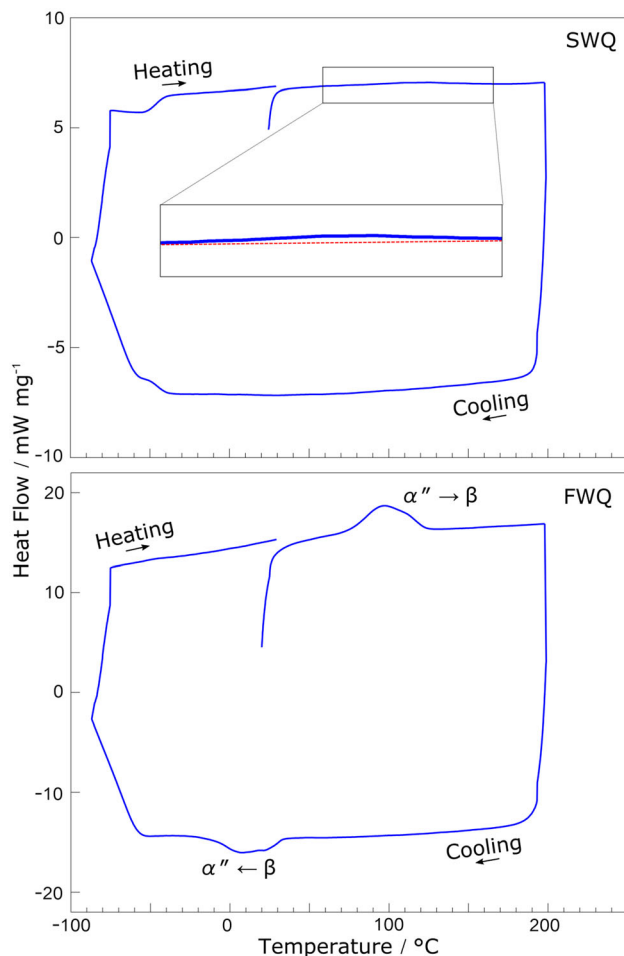


Fig. 6 DSC thermograms for the first complete heating/cooling cycle between 200 and -60 °C for the SWQ and FWQ conditions (exothermic down)

in Fig. 6. A very small thermal event was observed between 100 and 140 °C in the SWQ sample on heating, which was attributed to the small volume fraction of α'' reverting to the parent β phase. On cooling, there was no evidence of any thermal event. The changes in baseline close to -60 °C on both the heating and cooling segments of this curve were believed to be an artefact of the machine as they were also observed in non-transforming alloys subject to the same thermal cycle. This implies that the thermal cycle has had an effect on the propensity for α'' to form from the β phase. This effect was potentially quite dramatic, as the DSC cycle reached a much lower temperature than was initially obtained during the SWQ (-60 °C vs. 0 °C), meaning heating to 200 °C was sufficient to suppress M_s by at least 60 °C.

On heating the FWQ sample, a large thermal event was seen at a slightly lower temperature range of 80–120 °C. This was consistent with the much larger volume fraction of α'' observed in both the XRD and ECCI data. However, on cooling, a thermal event was also observed between 30 and -10 °C. It is believed that this corresponded to the transformation from β to α'' . This was significant, as the DSC heating and cooling rates were identical for both the FWQ and SWQ samples, yet these two material conditions displayed markedly different transformation behaviour. Consequently, this result implied that the initial cooling from the solution heat treatment must have altered the condition of the material.

As a single thermal cycle to 200 °C was sufficient to suppress M_s in the SWQ condition, these two samples were then cycled to progressively higher temperatures (Fig. 7), in order to elucidate the extent to which the peak temperature has an effect on this alloy. No subsequent thermal events were observed in the SWQ condition on either heating or cooling. In the FWQ condition, thermal events were apparent for both the heating and cooling segments of cycle 2, which reached a peak temperature of 250 °C, yet these peaks occurred at lower temperatures with respect to cycle 1. However, on cooling from 300 °C in cycle 3, there was no thermal event to indicate the re-formation of α'' . This suggested that on thermal cycling to progressively higher temperatures, the α'' phase was becoming increasingly less stable relative to the β phase, until it was no longer stable over the temperature range investigated. This variation of M_s temperature with cycle number is displayed in Fig. 8.

To ascertain whether the cause of this change in stability of the α'' phase was linked to the cyclic nature of the DSC run, or to the progressive increase in temperature, one sample in the FWQ condition was heated to a peak temperature of 300 °C; the first temperature where α'' did not reform on cooling, shown in Fig. 9, while another was cycled to 250 °C; the last peak temperature where the α'' to

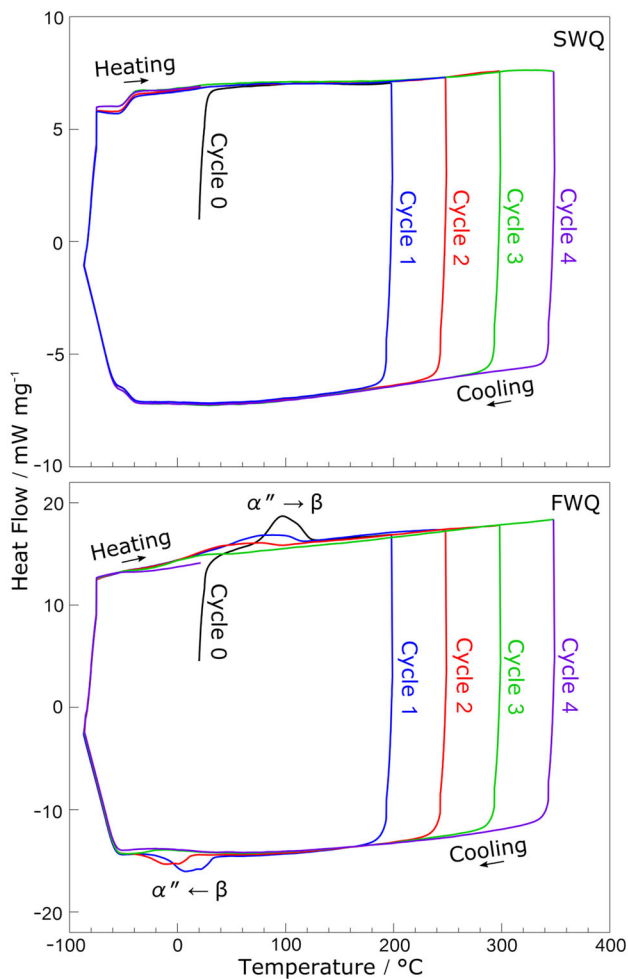


Fig. 7 DSC thermograms for the SWQ and FWQ conditions cycled to progressively higher temperatures. In cycle 0, the sample is heated to 200 °C. In cycle 1, the sample is cooled to – 60 °C and then heated to 250 °C. In cycles 2, 3 and 4, this is repeated, cooling to – 60 °C and then heating to peak temperatures of 250, 300 and 350 °C, respectively

β transformation still occurred on cooling and is displayed in Fig. 10.

The sample taken to 300 °C in a single cycle showed a thermal event on heating between 100 and 120 °C; however, on cooling, there was no evidence of any subsequent thermal event. The event that can be observed at – 20 °C was thought to be a baseline artefact, as similar events were also present in non-transforming alloys when subjected to the same cycle.

When cycled to 250 °C, thermal events were evident in both the heating and cooling segments of the cycle, around 100 °C and – 10 °C, respectively. As was seen in Fig. 7, these peaks shift to progressively lower temperatures with each cycle, indicating an increased stability of the β phase with respect to the α'' . The measured M_s temperature as a function of cycle number is presented in Fig. 11. An

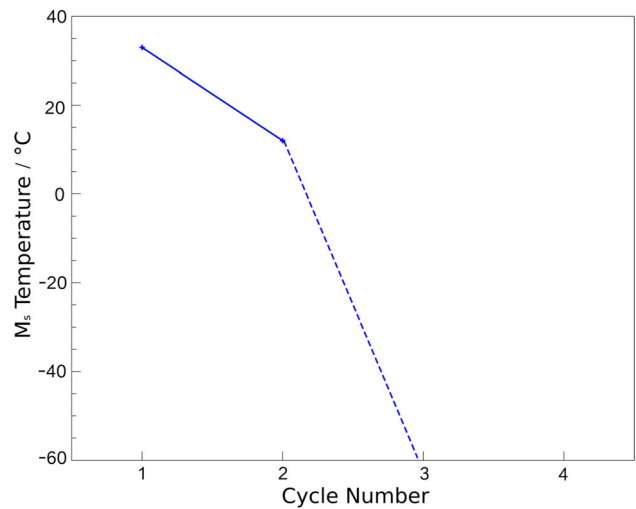


Fig. 8 M_s temperature as a function of cycle number for the FWQ condition. The solid line represents the observed decrease in M_s between cycles 1 and 2, and the dashed line represents an effective change in M_s , inferred from the lack of any transformation when cooling in cycle 3

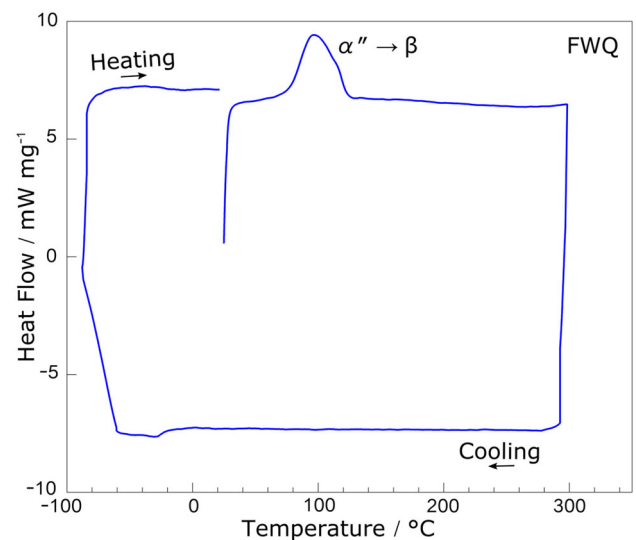


Fig. 9 DSC thermogram for the heating/cooling of a FWQ sample between 300 and – 60 °C

approximately linear relationship was observed. Note that the temperature at which the α'' reforms from the β phase in the first cycle was comparable to that in cycle 2 of Fig. 7, i.e. on cooling from 250 °C in both cases. Together this demonstrates that there was a temperature-dependant process causing a change in the condition of the material, which in turn decreased the stability of the α'' phase relative to the β . This process must have been active at 250 °C; however, it was much more prominent at 300 °C, further evidenced by the change in gradient with cycle number in Fig. 8.

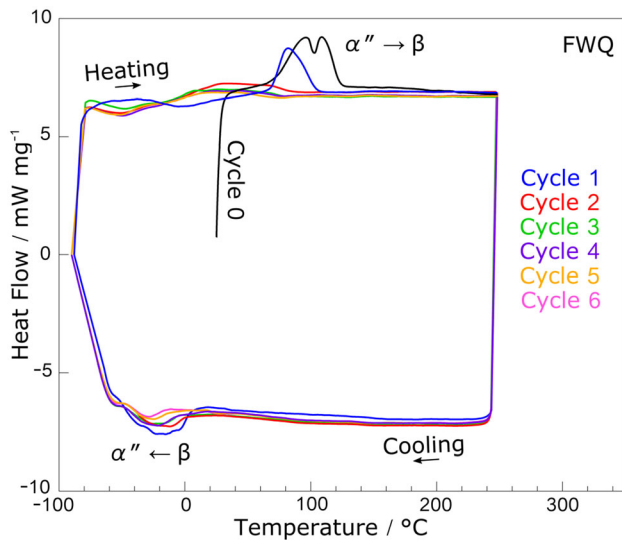


Fig. 10 DSC thermogram for multiple heating/cooling cycles of a FWQ sample between 250 and -60 °C

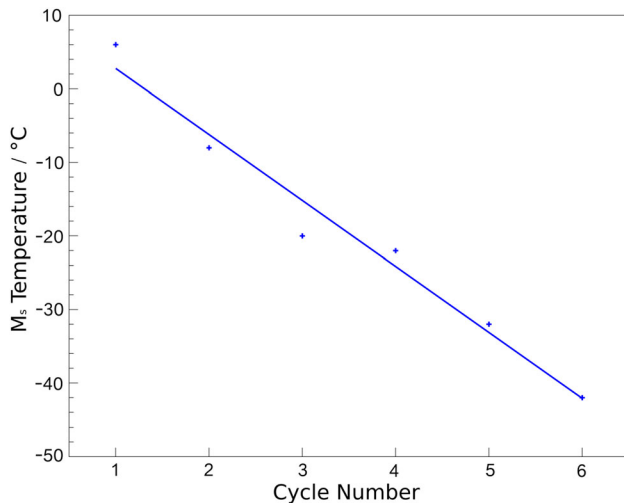


Fig. 11 Decrease in M_s observed as a function of cycle number for a sample in the FWQ condition cycled multiple times between 250 and -60 °C

As previous reports in the literature have linked a decrease in the M_s temperature with the formation of ω_{iso} , diffraction patterns and compositional mapping using STEM-EDX were obtained for the FWQ sample following heating to the peak temperature of 300 °C and cooling to room temperature in the DSC. These data are reported in Figs. 12 and 13, respectively. The diffraction data presented in Fig. 12 indicated that the material in this condition primarily consisted of the β phase. However, reflections characteristic of the ω phase were also present at $1/3$ and $2/3$ $\langle 112 \rangle_{\beta}$. In addition, weak intensity was also present at $1/2$ $\langle 112 \rangle_{\beta}$, potentially indicating the presence of the α'' martensite. However, no evidence of

martensitic features was observed when imaging the electron transparent regions of the foil. In addition, given the lack of signal in the corresponding thermogram, if the martensite phase is present, then it may as well be a result of damage incurred during ion beam milling.

To explore the nature of the ω phase present in this material, HAADF images and STEM-EDX data were obtained from the same region of the foil. As with the results presented for the AC condition above, some contrast was observed within the HAADF image, but no corresponding variations were present in the elemental distribution maps. Instead, the EDX data revealed an even distribution of the constituent elements. Consequently, these results suggest that the ω phase present in this condition must be the ω_{ath} form, as no evidence of a negative correlation between the Ti and Nb that would be expected for ω_{iso} was observed.

Discussion

The ECCI images presented in Fig. 1 clearly show that the microstructural condition of Ti2448 can vary dramatically when subjected to different cooling methods from the β phase field. The relatively slow cooled AC sample exhibited an entirely β microstructure, suggesting that M_s was below the quenching temperature of 0 °C. In contrast, the rapidly cooled FWQ condition contained a significant fraction of α'' , suggesting that M_s must have been elevated to above 0 °C. This point is supported by the DSC data presented in Fig. 6, where M_s was identified to be ~ 30 °C from the cooling segment and $A_s \sim 80$ °C from the heating segment of the FWQ sample data. As a consequence, room temperature lies below both the M_s and A_s transformation temperatures for material in this condition.

This observation has a significant implication for the likely mechanical behaviour of these samples, which will be related to their prior cooling rate. At room temperature for the FWQ condition, the martensitic transformation has not reached completion, hence a two-phase $\alpha'' + \beta$ microstructure exists. However, as can be seen in Fig. 1, a large proportion of the microstructure is martensitic. Thus, on loading, material in this condition can deform through two different mechanisms. Once σ_{SIM} has been reached, then the retained β will undergo a stress-induced transformation to α'' until the structure is entirely martensitic. However, the α'' formed during quenching will initially exist as twinned assemblies of martensite variants, so as to preserve the macroscopic shape of the material. Consequently, at a different critical stress, these variants will support macroscopic deformation through a detwinning process. Given that the vast majority of the initial microstructure is martensitic, detwinning would be

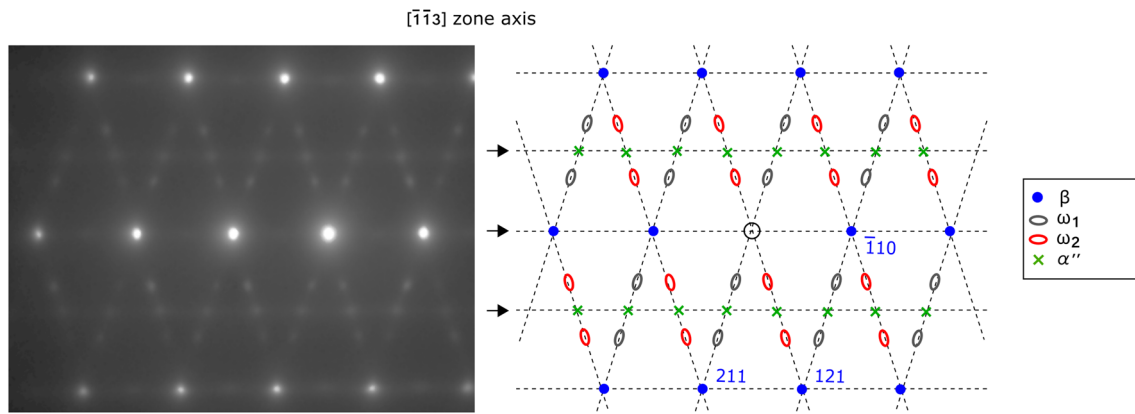


Fig. 12 TEM diffraction pattern of the FWQ condition, after heating and cooling to a peak temperature of 300 °C at 10 °C min⁻¹

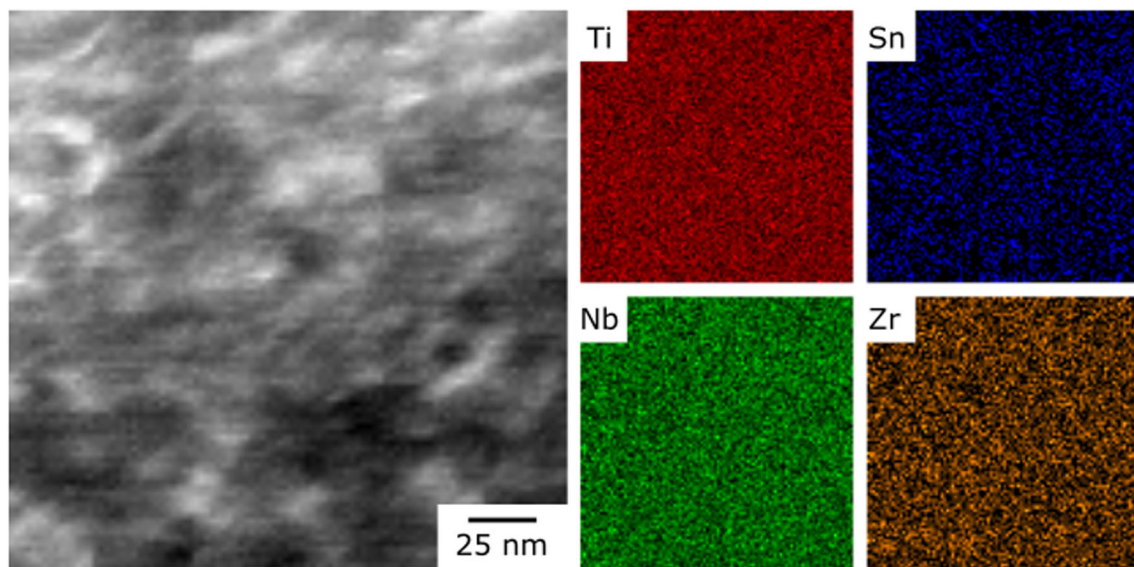


Fig. 13 HAADF image and STEM-EDX elemental distribution maps for Ti2448 in the FWQ condition, after heating and cooling to a peak temperature of 300 °C at 10 °C min⁻¹

expected to be the primary deformation mechanism. In contrast, there is minimal α'' in the initial microstructure of the SWQ condition material. Therefore, the predominant deformation mechanism will be the stress-induced transformation of β to α'' . Thus, the slight difference in cooling rate that leads to these two initial microstructural conditions also leads to different dominant deformation mechanisms and in all likelihood a different critical stress at which deformation begins. Irrespective of this difference, as the martensite is stable with respect to the β phase in both conditions, the deformation would not be recovered upon unloading.

Within the literature, Ti2448 in a comparable condition to the present AC condition showing complete superelastic recovery, implying both M_s and A_s (and the temperature at which the α'' to β transformation is complete, A_f) are below room temperature [40]. This dramatic difference in

mechanical behaviour is unexpected and highlights how small variations in the initial cooling must be influencing the observed transformation temperatures for this alloy. This point is further supported by the DSC thermograms in Figs. 6 and 7, which displayed different transformation temperatures for the SWQ and FWQ conditions on heating and cooling. In the SWQ condition, the martensite failed to reform on cooling during cycle 1, whereas in the FWQ condition, even after the α'' had reverted back to the parent β phase, the β to α'' transformation occurred again on cooling. While the transformation temperatures in the FWQ condition were seen to decrease and, therefore, approach those of the SWQ condition, this change occurs very slowly. Therefore, short thermal heat treatments may not be sufficient to reverse the effects of the initial processing. This is significant as it implies that the effect of the initial cooling method not only influences the starting

microstructures, but also effects the subsequent transformation behaviour over a number of thermal cycles.

In NiTi shape memory alloys, it has been observed that the defect concentration of a material has an impact on the M_s temperature [3–5]. In the present work, all samples were taken from the same starting stock, and subjected to identical solution treatments prior to cooling, to reduce the concentration of any defects present, such as dislocations. It follows that the defect concentration prior to the initial quench was comparable in all three conditions and hence not playing a role in the observed behaviour of the alloy in this case.

It is also well known that oxygen affects the propensity for the martensitic transformation, with an increase in oxygen decreasing the observed M_s temperature [37]. Both the AC and SWQ samples were heat treated and cooled under vacuum, while the FWQ sample did oxidise slightly when exposed to water during quenching. Therefore, the only sample that could have picked up any additional oxygen would be the FWQ condition. Oxygen pick-up would be expected to suppress the M_s temperature relative to the other two conditions, yet the FWQ condition demonstrated the highest M_s temperature of the three conditions considered. Therefore, the effect of oxygen has been disregarded as a potential driver for the observed behaviour.

Within the literature, the observation of much depressed M_s temperatures for alloys with identical composition has been linked to a refined grain size [32, 38]. In the present study, the grain size and texture were broadly consistent across all three microstructural conditions. Therefore, the behaviour reported here must be independent of composition, grain size and texture. Thus, the remaining variable that could influence the transformation behaviour of these samples is the way in which they were cooled from the solution heat treatment temperature.

Thermal cycles performed on material in the FWQ condition demonstrated a decrease in the M_s temperature, both as a result of higher peak temperatures being reached, and on cycling to the same temperature. Similar cyclic behaviour has been reported in a Ti-Mo base alloy, but this is the first commercial alloy in which such behaviour has been observed [16]. This is of significance as the re-formation of α'' in the FWQ condition after the first cycle suggests that α'' was thermodynamically more stable than the β phase at this temperature. Therefore, there must be another contributing factor, other than composition that was stabilising the α'' phase with respect to the β phase over this temperature range.

Other research groups have reported similar observations and proposed that this behaviour was related to the presence of ω_{iso} , which is known to form at the temperatures reached during the DSC runs [12, 13, 16]. ω_{iso} is believed to compete with the α'' and suppresses its

formation due to the diffusional enrichment of the matrix with β stabilising elements. Competition between α'' and ω was first reported for TiNb binary alloys cooled at three different rates [9]. For Ti20Nb, an alloy with comparable beta stability to the alloy studied here, α'' (but not ω) was present in the TEM diffraction data for a sample in the FWQ condition, whilst only ω was visible in both an AC and a furnace cooled (FC) sample. However, it should be noted that the cooling rate achieved will depend upon the specimen dimensions and, therefore, two air cooled samples cannot necessarily be assumed to be comparable. This point is highlighted by the STEM-EDX results presented in Fig. 4, which showed that the ω present in the initial microstructure of the AC condition sample was the ω_{ath} form. As such, it seems highly unlikely that the variation in subsequent transformation behaviour exhibited by the different condition samples studied here can be related to the formation of ω_{iso} .

Furthermore, samples of both the SWQ and FWQ condition material were subjected to a thermal cycle to 200 °C under identical heating and cooling profiles in the DSC. During the cooling segment of this cycle, the β to α'' transformation was observed in the FWQ condition material but not in the in the SWQ condition material, Fig. 6. For the conventional ω -based α'' suppression theory to rationalise this behaviour, a significant difference in the precipitation of the ω_{iso} phase would be required between these two conditions. This seems unlikely given that both the peak temperature and time spent heating and cooling was identical for the two tests.

Finally, the STEM-EDX data presented in Fig. 13 demonstrates that even after a thermal cycle to a peak temperature of 300 °C, during which the material spent 15 min within the rapid ω_{iso} precipitation window, no compositionally distinct features could be found. Consequently, it seems that within these short timeframes, ω_{iso} cannot form in this alloy and, therefore, the observed decrease in M_s temperature with thermal cycling, cannot be as a result of ω_{iso} precipitation.

An alternative theory has recently been proposed, which suggests that the observed microstructure is dependent on the total stress state of the material. This theory was developed for TiNb alloys in order to account for a large difference in M_s between samples of TiNb in different microstructural conditions [18].

Application of this new theory to the current results, does appear to rationalise the observed behaviours, if it is believed that the different cooling methods leads to thermal stresses of varying magnitude. It would be expected that the thermal stresses experienced by the FWQ condition are greater than those experienced by the SWQ and AC conditions. Thus during cooling, this stress is sufficient to initiate significant α'' formation in the FWQ condition, only

a little α'' in the SWQ condition and is insufficient to cause a transformation in the AC condition. In Ti2448, the β/α'' interface is irrational with a habit plane approximately 7.8° from $\{211\}_\beta$. Consequently, interfacial dislocations are required to maintain continuity at the boundary between phases [35]. Therefore, the formation of α'' will introduce dislocations into the FWQ material that are not present in the AC condition. These defects persist in the microstructure even after the α'' reverts to β and thus influence subsequent transformation behaviour.

When varying the peak temperature of a thermal cycle, the mobility of these defects changes and above a certain temperature they will be able to rearrange themselves, lowering the overall stress state within the material. In the SWQ sample, this results in the internal stress falling below σ_{SIM} for all of the temperatures investigated after just one cycle. However, the much higher initial stress state in the FWQ condition means that the β to α'' transformation can occur for multiple cycles or following heating to a greater peak temperature before the stress falls below σ_{SIM} . Further work is required to validate these arguments, but the total stress approach does appear to rationalise the behaviours observed in the current work, which was not possible through existing theories such as the formation of ω_{iso} .

Conclusion

The effect of three different cooling methods and thermal cycling on the microstructure of Ti2448 has been investigated. The microstructure and subsequent transformation behaviour has been shown to be highly sensitive to small variations in the rate at which the material is cooled from the β phase field. Faster cooling resulted in the formation of α'' , while material cooled at slower rates comprised β and ω . Thermal cycling of material in these different states revealed markedly different transformation behaviour and demonstrated a progressive depression of the M_s temperature. The observed behaviours cannot be rationalised by variations in composition, grain size or texture, nor were they consistent with the currently held theory of α'' suppression by ω_{iso} . Consequently, care must be taken when discussing the key transformation temperatures of these materials due to their clear dependence on prior processing, including cooling rates from a solution heat treatment.

Acknowledgements NLC would like to acknowledge support from the EPSRC and the Defence Science and Technology Laboratory through the provision of an Industrial CASE studentship.

Open Access This article is licensed under a Creative Commons Attribution 4.0 International License, which permits use, sharing, adaptation, distribution and reproduction in any medium or format, as

long as you give appropriate credit to the original author(s) and the source, provide a link to the Creative Commons licence, and indicate if changes were made. The images or other third party material in this article are included in the article's Creative Commons licence, unless indicated otherwise in a credit line to the material. If material is not included in the article's Creative Commons licence and your intended use is not permitted by statutory regulation or exceeds the permitted use, you will need to obtain permission directly from the copyright holder. To view a copy of this licence, visit <http://creativecommons.org/licenses/by/4.0/>.

Data Availability The underlying research data relating to this work can be accessed from The University of Cambridge repository (<https://doi.org/10.17863/CAM.64405>).

References

- Kim HY, Miyazaki S (2018) Ni-free Ti-based shape memory alloys. Elsevier, Amsterdam
- McMahon RE, Ma J, Verkhoturov SV et al (2012) A comparative study of the cytotoxicity and corrosion resistance of nickel-titanium and titanium-niobium shape memory alloys. *Acta Biomater* 8:2863–2870
- Sedmák P, Šittner P, Pilch J, Curfs C (2015) Instability of cyclic superelastic deformation of NiTi investigated by synchrotron X-ray diffraction. *Acta Mater* 94:257–270
- Srivastava AK, Schryvers D, Van Humbeeck J (2007) Grain growth and precipitation in an annealed cold-rolled Ni50.2Ti49.8 alloy. *Intermetallics* 15:1538–1547
- Waitz T, Kazykhanov V, Karnthaler HP (2004) Martensitic phase transformations in nanocrystalline NiTi studied by TEM. *Acta Mater* 52:137–147
- Kim HY, Ohmatsu Y, Kim JI et al (2004) Mechanical properties and shape memory behavior of Ti-Nb alloys. *Mater Trans* 45:1090–1095
- Kim HY, Hashimoto S, Kim JI et al (2006) Effect of Ta addition on shape memory behavior of Ti-22Nb alloy. *Mater Sci Eng A* 417:120–128
- Kim JI, Kim HY, Inamura T et al (2005) Shape memory characteristics of Ti-22Nb-(2–8)Zr(at.%) biomedical alloys. *Mater Sci Eng A* 403:334–339
- Moffat DL, Larbalestier DC (1988) Competition between martensite and omega in quenched TiNb alloys. *Metall Trans A Phys Metall Mater Sci* 19:1677–1686
- Lai MJ, Li T, Raabe D (2018) Ω phase acts as a switch between dislocation channeling and joint twinning- and transformation-induced plasticity in a metastable B titanium alloy. *Acta Mater* 151:67–77
- Chen W, Cao S, Kou W et al (2019) Origin of the ductile-to-brittle transition of metastable β -titanium alloys: self-hardening of ω -precipitates. *Acta Mater* 170:187–204
- Buenconsejo PJS, Kim HY, Hosoda H, Miyazaki S (2009) Shape memory behavior of Ti-Ta and its potential as a high-temperature shape memory alloy. *Acta Mater* 57:1068–1077
- Kim HY, Fukushima T, Buenconsejo PJS et al (2011) Martensitic transformation and shape memory properties of Ti-Ta-Sn high temperature shape memory alloys. *Mater Sci Eng A* 528:7238–7246
- Pang E (2016) The effect of zirconium additions on phase stability in metastable beta titanium niobium alloys, MPhil Thesis. University of Cambridge Library, Cambridge
- Takahashi E, Sakurai T, Watanabe S et al (2002) Effect of heat treatment and Sn content on superelasticity in biocompatible TiNbSn alloys. *Mater Trans* 43:2978–2983

16. Al-Zain Y, Kim HY, Hosoda H et al (2010) Shape memory properties of Ti-Nb-Mo biomedical alloys. *Acta Mater* 58:4212–4223
17. Wang CH, Liu M, Hu PF et al (2017) The effects of α'' and ω phases on the superelasticity and shape memory effect of binary Ti-Mo alloys. *J Alloys Compd* 720:488–496
18. Hildyard EM, Connor LD, Owen LR et al (2020) The influence of microstructural condition on the phase transformations in Ti-24Nb (at.%). *Acta Mater* 199:129–140
19. Sun F, Nowak S, Gloriant T et al (2010) Influence of a short thermal treatment on the superelastic properties of a titanium-based alloy. *Scr Mater* 63:1053–1056
20. Sun F, Zhang JY, Marteleur M et al (2013) Investigation of early stage deformation mechanisms in a metastable β titanium alloy showing combined twinning-induced plasticity and transformation-induced plasticity effects. *Acta Mater* 61:6406–6417
21. Talling RJ, Dashwood RJ, Jackson M, Dye D (2009) On the mechanism of superelasticity in Gum metal. *Acta Mater* 57:1188–1198
22. Vorontsov VA, Jones NG, Rahman KM, Dye D (2015) Superelastic load cycling of Gum Metal. *Acta Mater* 88:323–333
23. Jones NG, Vorontsov VA, Dye D (2016) The behaviour of GUM metal (Ti-36Nb-2Ta-3Zr-0.3O wt.%) during superelastic cycling. TMS. Wiley, Hoboken, pp 899–904
24. Yang R, Hao YL, Li SJ (2011) Development and application of low-modulus biomedical titanium alloy Ti2448. *Biomed Eng Trends Mater Sci* 10:225–248
25. Yang Y, Castany P, Cornen M et al (2014) Texture investigation of the superelastic Ti-24Nb-4Zr-8Sn alloy. *J Alloys Compd* 591:85–90
26. Hao YL, Zhang ZB, Li SJ, Yang R (2012) Microstructure and mechanical behavior of a Ti-24Nb-4Zr-8Sn alloy processed by warm swaging and warm rolling. *Acta Mater* 60:2169–2177
27. Hao YL, Li SJ, Sun SY et al (2007) Elastic deformation behaviour of Ti-24Nb-4Zr-7.9Sn for biomedical applications. *Acta Biomater* 3:277–286
28. Li SJ, Jia MT, Prima F et al (2011) Improvements in nonlinear elasticity and strength by grain refinement in a titanium alloy with high oxygen content. *Scr Mater* 64:1015–1018
29. Li SJ, Cui TC, Li YL et al (2008) Ultrafine-grained β -type titanium alloy with nonlinear elasticity and high ductility. *Appl Phys Lett* 92:043128
30. Yang Y, Castany P, Cornen M et al (2015) Characterization of the martensitic transformation in the superelastic Ti-24Nb-4Zr-8Sn alloy by in situ synchrotron X-ray diffraction and dynamic mechanical analysis. *Acta Mater* 88:25–33
31. Hao YL, Li SJ, Sun SY, Yang R (2006) Effect of Zr and Sn on Young's modulus and superelasticity of Ti-Nb-based alloys. *Mater Sci Eng A* 441:112–118
32. Hao YL, Li SJ, Prima F, Yang R (2012) Controlling reversible martensitic transformation in titanium alloys with high strength and low elastic modulus. *Scr Mater* 67:487–490
33. Wang HL, Hao YL, He SY et al (2017) Elastically confined martensitic transformation at the nano-scale in a multifunctional titanium alloy. *Acta Mater* 135:330–339
34. Coakley J, Isheim D, Radecka A et al (2017) Microstructural evolution in a superelastic metastable beta-Ti alloy. *Scr Mater* 128:87–90
35. Obbard EG, Hao YL, Talling RJ et al (2011) The effect of oxygen on α'' martensite and superelasticity in Ti-24Nb-4Zr-8Sn. *Acta Mater* 59:112–125
36. Wei LS, Kim HY, Miyazaki S (2015) Effects of oxygen concentration and phase stability on nano-domain structure and thermal expansion behavior of Ti-Nb-Zr-Ta-O alloys. *Acta Mater* 100:313–322
37. Kim HY, Miyazaki S (2015) Martensitic transformation and superelastic properties of Ti-Nb base alloys. *Mater Trans* 56:625–634
38. Hao YL, Niinomi M, Kuroda D et al (2002) Young's modulus and mechanical properties of Ti-29Nb-13Ta-4.6Zr in relation to α'' martensite. *Metall Mater Trans A Phys Metall Mater Sci* 33:3137–3144
39. Kim HY, Sasaki T, Okutsu K et al (2006) Texture and shape memory behavior of Ti-22Nb-6Ta alloy. *Acta Mater* 54:423–433
40. Coakley J, Rahman KM, Vorontsov VA et al (2016) Effect of precipitation on mechanical properties in the β -Ti alloy Ti-24Nb-4Zr-8Sn. *Mater Sci Eng A* 655:399–407

Publisher's Note Springer Nature remains neutral with regard to jurisdictional claims in published maps and institutional affiliations.